The Journal of Immunology

TNFR1/Phox Interaction and TNFR1 Mitochondrial Translocation Thwart Silica-Induced Pulmonary Fibrosis

Fabrizio Fazzi, Joel Njah, Michelangelo Di Giuseppe, Daniel E. Winnica, Kristina Go, Ernest Sala, Claudette M. St Croix, Simon C. Watkins, Vladimir A. Tyurin, Donald G. Phinney, Cheryl L. Fattman, George D. Leikauf, Valerian E. Kagan and Luis A. Ortiz

J Immunol 2014; 192:3837-3846; Prepublished online 12 March 2014;
doi: 10.4049/jimmunol.1103516
http://www.jimmunol.org/content/192/8/3837

The Journal of Immunology is published twice each month by
The American Association of Immunologists, Inc.,
1451 Rockville Pike, Suite 650, Rockville, MD 20852

Print ISSN: 0022-1767 Online ISSN: 1550-6606.

TNFR1/Phox Interaction and TNFR1 Mitochondrial Translocation Thwart Silica-Induced Pulmonary Fibrosis

Fabrizio Fazzi,*,[1] Joel Njah,*,[1] Michelangelo Di Giuseppe,* Daniel E. Winnica,* Kristina Go,* Ernest Sala,* Claudette M. St Croix,*,† Simon C. Watkins,† Vladimir A. Tyurin,*,‡ Donald G. Phinney,§ Cheryl L. Fattman,* George D. Leikauf,* Valerian E. Kagan,*,‡ and Luis A. Ortiz*

Macrophages play a fundamental role in innate immunity and the pathogenesis of silicosis. Phagocytosis of silica particles is associated with the generation of reactive oxygen species (ROS), secretion of cytokines, such as TNF, and cell death that contribute to silica-induced lung disease. In macrophages, ROS production is executed primarily by activation of the NADPH oxidase (Phox) and by generation of mitochondrial ROS (mtROS); however, the relative contribution is unclear, and the effects on macrophage function and fate are unknown. In this study, we used primary human and mouse macrophages (C57BL/6, BALB/c, and $p47^{phox-/-}$) and macrophage cell lines (RAW 264.7 and IC21) to investigate the contribution of Phox and mtROS to silica-induced lung injury. We demonstrate that reduced $p47^{phox}$ expression in IC21 macrophages is linked to enhanced mtROS generation, cardiolipin oxidation, and accumulation of cardiolipin hydrolysis products, culminating in cell death. mtROS production is also observed in $p47^{phox-/-}$ macrophages, and $p47^{phox-/-}$ mice exhibit increased inflammation and fibrosis in the lung following silica exposure. Silica induces interaction between TNFR1 and Phox in RAW 264.7 macrophages. Moreover, TNFR1 expression in mitochondria decreased mtROS production and increased RAW 264.7 macrophage survival to silica. These results identify TNFR1/Phox interaction as a key event in the pathogenesis of silicosis that prevents mtROS formation and reduces macrophage apoptosis. ***The Journal of Immunology*****, 2014, 192: 3837–3846.**

Inhalation of crystalline silica leads to the development of silicosis, a progressive pneumoconiosis associated with autoimmune diseases, mycobacterial infection, and lung cancer. Exposure to silica is common; >2 million people are exposed to silica in the United States every year, and silicosis remains a global threat for which no specific therapy is available (1).

The innate immune response is fundamental to the development of silicosis (2–4). Macrophages phagocytose silica particles into phagosomes during the internalization process (5). Subsequently, macrophages experience phagosomal destabilization and release inflammatory cytokines (4, 6, 7). In contrast to microorganisms, silica particles cannot be degraded; macrophages undergo cell death, releasing these particles that are engulfed by other macrophages, thus perpetuating inflammation (4).

Reactive oxygen species (ROS) are essential components of the innate immune response and are involved in cytokine production, microbial clearance, cell proliferation, and death (8). In macrophages, ROS production is initiated primarily by activation of the NADPH oxidase (Phox) and by generation of mitochondrial ROS (mtROS); however, the relative contribution of each is unclear, and the effects on macrophage function and fate are unknown (9). Engagement of TLRs in macrophages results in recruitment of mitochondria to phagosomes and mtROS production that contribute to the bactericidal activity of macrophages (10). $p47^{phox}$ deficiency impairs macrophage ability to clear bacteria and leads to exacerbated lung inflammation and increased mortality to a variety of agents (11–13). Inflammatory changes in $p47^{phox}$-deficient ($p47^{phox-/-}$) mice occur, despite a reduced ability of $p47^{phox-/-}$ macrophages to activate NF-κB (14). The effects of silica on macrophage Phox are poorly understood; based on the above data, it is possible that silica-induced lung inflammation could be exacerbated by reduced macrophage Phox expression.

ROS triggers TNF production in silica-exposed macrophages (15). TNF plays a fundamental role in silicosis and activates the NADPH oxidase in fibroblasts via TNFR1 (16–18). TNF dually mediates resistance and susceptibility to intracellular pathogens, such as mycobacteria, by promoting mtROS generation (19, 20). The contribution of mtROS to the observed inflammatory activity of $p47^{phox}$-deficient macrophages is not known. In HeLa cells, TNFR1 activation of NADPH involves the recruitment of riboflavin kinase (RFK) to the death domain of the receptor, where it is coupled to the $p22^{phox}$ subunit of the oxidase (21). The mechanisms by which TNF induces mtROS production are poorly understood, but TNFR1 translocation to mitochondria could play

*Department of Environmental and Occupational Health, University of Pittsburgh, Pittsburgh, PA 15219; †Department of Cell Biology, University of Pittsburgh, Pittsburgh, PA 15219; ‡Center for Free Radical and Antioxidant Health, University of Pittsburgh, Pittsburgh, PA 15219; and §The Scripps Research Institute, Jupiter, FL 33458

[1]F.F. and J.N. contributed equally to this work.

Received for publication December 6, 2011. Accepted for publication February 9, 2014.

This work was supported in part by U.S. Public Health Service Grants ES10859 and ES015675 from the National Institutes of Environmental Health (to L.A.O. and G.D.L.) and Grant HL085655 from the National Heart, Lung, and Blood Institute (to G.D.L).

Address correspondence and reprint requests to Dr. Luis A. Ortiz, Division of Occupational and Environmental Medicine, Graduate School of Health at the University of Pittsburgh, Bridgeside Point, 100 Technology Drive, Suite 557, Pittsburgh, PA 15219. E-mail address: LAO1@Pitt.edu

The online version of this article contains supplemental material.

Abbreviations used in this article: BID, BH3 interacting death domain agonist; CL, cardiolipin; CLox, oxidized CL; MLCL, monolysocardiolipin; MP, microperoxidase; MS, mass spectrometry; mtROS, mitochondrial reactive oxygen species; RFK, riboflavin kinase; ROS, reactive oxygen species; shRNA, short hairpin RNA.

a role, and cells with mutations in TNFR1 exhibit increased mtROS (22, 23). TNF-induced mtROS has been linked to cell death by promoting mitochondrial permeability transition pore formation, cardiolipin (CL) migration to the outer mitochondrial membrane, and cytochrome *c* mobilization into the cytosol (20, 24).

The purpose of the current study was to determine the role of Phox in silica-induced lung inflammation and fibrosis. We investigated whether silica exposure alters Phox macrophage expression and whether TNFR1/Phox and mtROS generation constitute an integral aspect of the macrophage response to silica. To address these questions, we studied the expression of Phox proteins in macrophage cell lines, as well as in primary human and mouse macrophages. We used advanced proteomics and live microscopy to document the TNFR1/Phox interaction, TNFR1 mitochondrial translocation, and the real-time generation of mtROS in silica-exposed macrophages. We conducted proteomic analysis to document potential protein interactions between the translocated TNFR1 and mitochondrial proteins. Finally, we confirmed and enhanced mtROS production in silica-exposed $p47^{phox-/-}$-deficient macrophages and demonstrated an enhanced sensitivity of $p47^{phox-/-}$ mice to silica.

Materials and Methods

Reagents

Goat polyclonal anti-TNFR1 (p55) (sc-1069[G-20], sc-1070[E-20]), anti-TRADD (sc-1164), anti-Bid (sc-11423, 6291, RAW 264.7 whole-cell lysate 2211), anti-RFK (sc-67308), anti-$p22^{phox}$ (sc-20781), anti-$p47^{phox}$ (sc-7760), gp91 (sc-130543), anti-caspase 8 p20 (sc-6134,6135,7890), anti-GAPDH (sc-25778), and anti-goat polyclonal anti-hamster IgG peroxidase-conjugated Abs were purchased from Santa Cruz Biotechnology (Santa Cruz, CA). Anti–caspase 8 p43/p18, anti–cytochrome *c*, and anti-$p67^{phox}$ were purchased from Cell Signaling Technology, anti-caspase 8DED was purchased from Becton Dickinson Biotechnology, and anti-GAPDH and β-actin were purchased from Sigma-Aldrich. Hamster monoclonal anti-mouse TNFR1 (p55) Ab (clone 55R-286), propidium iodide stain, and Annexin V–FITC were obtained from BD Pharmingen (San Diego, CA). Polyclonal rabbit anti-goat Igs/HRP were purchased from DAKO (Carpinteria, CA).

Macrophage exposure to silica

Mouse macrophages were isolated from the bone marrow of C57BL/6 or BALB/c mice, as previously described (25). Human macrophages were derived from monocytes isolated from the mononuclear cell layer of leukapheresis packs, as previously described (26). The mouse macrophage cell lines IC21 and RAW 264.7 were purchased from the American Type Culture Collection (Rockville, MD) and cultured in RPMI 1640 medium (Life Technologies BRL, Rockville, MD) supplemented with 10% FBS, 100 U/ml penicillin G, and 100 μg/ml streptomycin and grown at 37°C in 5% CO_2. Crystalline silica (α-quartz; average size, 1.7 μm) was obtained from U.S. Silica (Berkeley Springs, WV). It was selected by sedimentation, according to Stokes' law, acid hydrolyzed, and baked overnight (200°C, 16 h) to inactivate endotoxin contamination.

Silencing $p47^{phox}$ in IC21 macrophages

IC21 macrophages were infected with $p47^{phox}$-specific short hairpin RNA (shRNA) lentiviral particles or shRNA plasmids (Santa Cruz Biotechnology), following the manufacturer's directions. Briefly, 1×10^6 IC21 cells were transfected with 100 μl lentiviral particle–containing solution in RPMI 1640 medium containing 5 μg/ml Polybrene, and cells were incubated overnight at 37°C in 5% CO_2. shRNA $p47^{phox}$ IC21 clones were selected by their resistance to puromycin (Sigma-Aldrich) and subsequently expanded for further experimentation. Western blotting confirmed reduced $p47^{phox}$ expression with the use of anti-$p47^{phox}$ (sc-7760; Santa Cruz Biotechnology).

Silica treatment

The Institutional Animal Care and Use Committee of the University of Pittsburgh approved all procedures. Specific pathogen–free female C57BL/6 mice (Charles River Laboratories, Kingston, NY) and mice genetically deficient in $p47^{phox}$ (Taconic), weighing 20–25 g, were housed in pathogen-free cabinets, as previously described (11).

Macrophage production superoxide anion was assayed measuring cytochrome c reduction in silica-exposed macrophages. A total of 1×10^5 macrophages was seeded in 96-well microplates overnight before treatment. The reaction medium contained 100 μM cytochrome *c*; 20 $\mu g/cm^2$ silica particles suspended in PBS (pH 7.4) was added to cell cultures and placed in a 5% CO_2 incubator at 37°C for up to 6 h. Absorbance was measured (550 nm) using a microplate reader. The amount of reduced cytochrome *c* is expressed as nmol/μg protein. The basal level of cytochrome *c* reduction in untreated cells was subtracted from the silica-exposed values for comparison of data.

Live cell imaging of mtROS generation

Cells were seeded on 35-mm laminin-coated glass-bottom dishes (MatTek, Ashland, MA) and incubated with 5 μM MitoSOX Red mitochondrial superoxide indicator (Invitrogen, Eugene, OR) for 15 min at 37°C. Mitochondrial localization was confirmed using MitoTracker Green (Invitrogen). Cells were washed with PBS, the media were replaced, and the dish was inserted in a closed, thermo-controlled (37°C) stage top incubator (Tokai-Hit, Tokyo, Japan). Images were obtained using a Nikon TE2000E microscope equipped with a 60× oil-immersion objective (Nikon, CFI Plan Fluor, NA 1.43). Emission imaging was performed using a DsRed and FITC Longpass filter set (Chroma, Rockingham, VT) and collected with a Q-Imaging Retiga EXI camera (Burnaby, BC, Canada) and MetaMorph software (Molecular Devices, Downington, PA). For each experiment, images were collected from a minimum of six cells in each of 10 stage positions, for a minimum of three subcultures of cells.

RT-PCR

Following silica exposure, RNA from 2×10^6 RAW 264.7, IC21, C57BL/6, or $p47^{phox-/-}$ macrophages was extracted with TRI Reagent (Sigma-Aldrich), according to the manufacturer's protocol. One microgram of RNA was converted into cDNA using the iScript cDNA Synthesis Kit (Bio-Rad) and probed for $p47^{phox}$ gene expression using TaqMan (Applied Biosystems)–specific transcripts mapping exon 1 (Mm00447915_m1) and exon 7 (Mm00447920_g1). PCR reactions were conducted on a PCR instrument (Applied Biosystems 7900). Results are expressed as Δct using the Ct value of RPL32 (Mm02528467_g1) expression as housekeeping gene (exon 1) or the values obtained from $p47^{phox-/-}$ macrophages (exon 7) as calibrator. To determine in vivo expression of inflammatory and fibrotic genes, RNA (1 μg) isolated from the left lung of control or silica-exposed mice was converted into cDNA, and expression of TNF-α (Mm00443258_m1), TGF-β (Mm01178820_m1), IL-6 (Mm00446190_m1), α(I) collagen (Mm00801666_g1) transcripts was quantified by TaqMan gene expression using RPL32 (Mm02528467_g1) gene expression as internal control.

Detection of cell death

Cell death was analyzed by evaluating (flow cytometry) annexin V binding and the exclusion of propidium iodide by macrophages, as previously described (27).

TNFR1 immunoprecipitation and isolation of caveolae-enriched membrane fractions

Immune precipitation of TNFR1 and isolation of caveolae-enriched membrane fractions were conducted using modifications of previously described protocols (21).

Mitochondrial membrane potential in silica-exposed macrophages

To measure mitochondrial membrane potential, silica-exposed (20 $\mu g/cm^2$) IC21 and RAW 264.7 macrophages were incubated with 5 mM JC-1 in HBSS at 37°C for 30 min and by following FACS to measure JC-1 monomers and aggregates. A 488-nm excitation line from an argon laser was used in conjunction with a 510-nm dichroic mirror. A 575-nm dichroic mirror separated emitted light further before being filtered at 530 and 590 nm, the wavelengths corresponding to the peak fluorescence from the monomer and aggregate signals, respectively, of the dye JC-1. The fluorescence ratios (indicative of membrane potential) were determined for each time point at 1-min intervals.

Complex I isolation and enzymatic assay

Complex I was isolated from silica-exposed macrophages with a Complex I Immunocapture Kit (MitoSciences), which uses a mAb irreversibly cross-linked to protein G–agarose beads to immunocapture Complex I. Mitochondrial Complex I activity was measured spectrophotometrically (DU-530;

Beckman Coulter). Mitochondrial pellets were lysed in potassium/phosphate buffer (pH 8) containing NADH (100 μM), ubiquinone-2 (50 μM), a phospholipid supplement (0.005% n-Dodecyl-β-D-Maltopyranoside from Anatrace), and 200 μg protein from the mitochondrial pellet by following the oxidation of NADH at 340 nm initiated by ubiquinone-2. Data were acquired every 5 s for 5 min after initiation of the reaction, and every 2 min following the addition of rotenone (20 μM), to inhibit electron transfer from iron-sulfur centers in Complex I to ubiquinone.

CL hydroperoxides were determined by fluorescence HPLC of products formed in microperoxidase (MP)-11–catalyzed reaction with a fluorogenic substrate, Amplex Red (*N*-Acetyl-3,7-dihydroxyphenoxazine; Molecular Probes, Eugene, OR). Oxidized CL was hydrolyzed by porcine pancreatic phospholipase A2 (2 U/μl) in 25 mM phosphate buffer containing 1.0 mM Ca, 0.5 mM EDTA, and 0.5 mM SDS ([pH 8] at room temperature for 30 min). Subsequently, 50 μM Amplex Red and MP-11 (1.0 μg/μl) were added, and samples were incubated at 4°C for 40 min. The reaction was terminated by addition of 100 μl stop reagent (10 mM HCl, 4 mM BHT in ethanol). After centrifugation at 15,000 × *g* for 5 min, aliquots of supernatant (5 μl) were injected into an Eclipse XDB-C18 column (5 μm, 150 × 4.6 mm). The mobile phase was composed of 25 mM KH_2PO_4 (pH 7.0)/methanol (60:40 v/v). The flow rate was 1 ml/min. Resorufin (an Amplex Red oxidation product) fluorescence was measured at 590 nm after excitation at 560 nm using a Shimadzu LC-100AT vp HPLC system equipped with a fluorescence detector (RF-10AXL) and autosampler (SIL-10ADVP). Data were processed and stored in digital form using Class-VP software.

Two-dimensional difference gel electrophoresis

A total of 50 mg macrophage-derived protein from each sucrose gradient (4–6) sample was labeled with Cy3 or Cy5 minimal dyes, and the pooled internal standard was labeled with Cy2 in the dark. The labeled protein samples were multiplexed to run two analytical samples and one internal standard on each gel. Labeled protein was brought to a volume of 450 ml in rehydration buffer containing 20 mM DTT and 0.05% (v/v) carrier ampholytes (pH 4–7) (GE Healthcare). A 24-cm linear pH 4–7 immobilized pH gradient strip was immersed in each solution. The first-dimensional separation of proteins was performed using an IPGphor 3 U (GE Healthcare), with the following settings: 30 V for 12 h for the rehydration step, then 200 V for 1 h, 500 V for 1 h, 1,000 V for 1 h, and then a gradient to 8,000 V over 3 h, to a total of 50,000 V-hours, according to the manufacturer's instructions. After isoelectric focusing, the strips were equilibrated in sample buffer containing 100 mg DTT and then 250 mg iodoacetamide. The equilibrated strips were placed onto 12% $NaDodSO_4$ gels (Jule gels). The second dimension was performed using an Ettan DALT six (GE Healthcare) run at 2 W/gel. The samples were assessed in two separate gel runs, resulting in 12 gels (36 gel images), and each pooled sample was represented in 6 images.

The two-dimensional gels were scanned using the Typhoon 9400 Imager (GE Healthcare). The resulting gel images were imported into DeCyder v5.02 software (GE Healthcare), which outputs a list of statistically significant differences in protein expression, including *t* test values, using the Cy2 internal standard. Both differential in-gel analysis, which includes codetection, background subtraction, normalization, and quantization of spots in an image pair, as well as biologic variation analysis, which matches multiple gels for comparison and statistical analysis of protein abundance changes, were used in this analysis. Spot features that were significantly differentially expressed ($p < 0.05$ by unpaired *t* test and >2-fold the average ratio) in each comparison and that were present on 75% of all spot maps were chosen for further investigation. Each spot identified as significantly differentially expressed was manually assessed to ensure that only true protein spots were picked.

In-gel protein digestion and identification

A preparative gel that contained 450 μg unlabeled pooled internal standard was run using the same conditions as for the analytical gels (as described above), stained with Deep Purple protein stain (GE Healthcare), and matched to the analytical gels in biologic variation analysis. The Ettan Spot Handling Workstation (GE Healthcare) was used for the preparative gel spot picking, tryptic digestion, and spotting onto a MALDI plate that was subsequently analyzed by MALDI-TOF/TOF (ABI 4800). The same spots also were analyzed on the LC/quadrupole-TOF MS system for peptide sequence information. The mass spectrometry (MS) and tandem MS data were searched against the NCBInr and Swiss-Prot protein databases.

Statistics

The results are presented as mean ± SD from at least three experiments, and statistical analyses were performed using the Student *t* test or one-way ANOVA. A Student *t* test was used to estimate the significance of differences in the accumulation of phospholipid hydroperoxides by Amplex Red procedure in lipids extracted from silica-exposed macrophages. In experiments with cells and animals, the significance of differences was estimated by one-way or multiple-way ANOVA to assess the difference among strains and treatment. The statistical significance of differences was set at $p < 0.05$.

Results

Silica reduces p47^{phox} expression in macrophages

To study ROS production in response to silica, we selected the RAW 264.7 and IC21 macrophage cell lines that exhibit well-characterized differences in cell death in response to silica (27). Silica induces a rapid and sustained production of superoxide anion by RAW 264.7 and IC21 macrophages, and this response is greater in IC21 macrophages compared with RAW 264.7 macrophages (Fig. 1A). Differences in superoxide anion production between these cells also were observed in response to other agents, such as PMA (Fig. 1A).

In macrophages, Phox consists of five subunits; under basal conditions, p40^{phox}, p47^{phox}, and p67^{phox} are located in the cytosol, whereas p22^{phox} and gp91^{phox} are membrane bound and form the cytochrome b_{558} complex (8). Following cell stimulation, the p47^{phox} subunit is phosphorylated, and the complex migrates to the membrane where it associates with cytochrome b_{558} to form the active NADPH oxidase (8). Baseline levels of Phox proteins were similar in IC21 and RAW 264.7 macrophage (Fig. 1B). However, in response to silica, p47^{phox} protein expression was decreased in IC21, but not RAW 264.7, macrophages (Fig. 1B). Reduced expression of p47^{phox} protein was associated with a time-dependent decrease in the expression of mRNA encoding exons 1 and 7 of the p47^{phox} protein (Supplemental Fig. 1).

To determine whether the effect of silica particles on p47^{phox} protein expression was observed in primary macrophages, we isolated macrophages from the bone marrow of C57BL/6J and BALB/c mice, which constitute the genetic strain backgrounds from which IC21 and RAW 264.7 cells are derived, respectively, or we differentiated human monocytes, isolated from peripheral blood of normal human subjects, into macrophages. Similar to the IC21 macrophages, those isolated from the bone marrow of C57BL/6J mice exhibited a significantly decreased p47^{phox} protein expression (2–4 h) in response to silica (Fig. 1B). In contrast, no decrease in p47^{phox} protein expression was observed in BALB/c macrophages after silica exposure (Fig. 1B). Similar to mouse macrophages, silica exposure decreased p47^{phox} protein expression in human macrophages, although the reduction was observed at later (4–8 h) times (Fig. 1B). Therefore, RAW 264.7 and IC21 cells reflect the biology of primary macrophages and constitute a valid model with which to study the effect of silica on these cells.

Mitochondria: a significant source of ROS in silica-exposed macrophages

Use of mitochondrial-specific superoxide (fluorogenic) reporter (MitoSOX) allows for the real-time evaluation of mitochondrial superoxide anion production by silica-stimulated RAW 264.7 or IC21 macrophages (Fig. 1C). Superoxide anion production is negligible in resting nonstimulated macrophages; however, mitochondrial superoxide anion production increased in both macrophage cell lines following exposure to silica but was significantly greater in IC21 macrophages. Increases in mitochondrial-associated fluorescence occurred within 1 h and peaked 3 h after silica exposure (Fig. 1C; the dynamics of the uptake of silica by MitoSOX-labeled IC21 macrophages and the subsequent production of superoxide are included in Supplemental Video 1). Similar to IC21 macrophages, p47$^{phox-/-}$ macrophages significantly increased mitochondrial su-

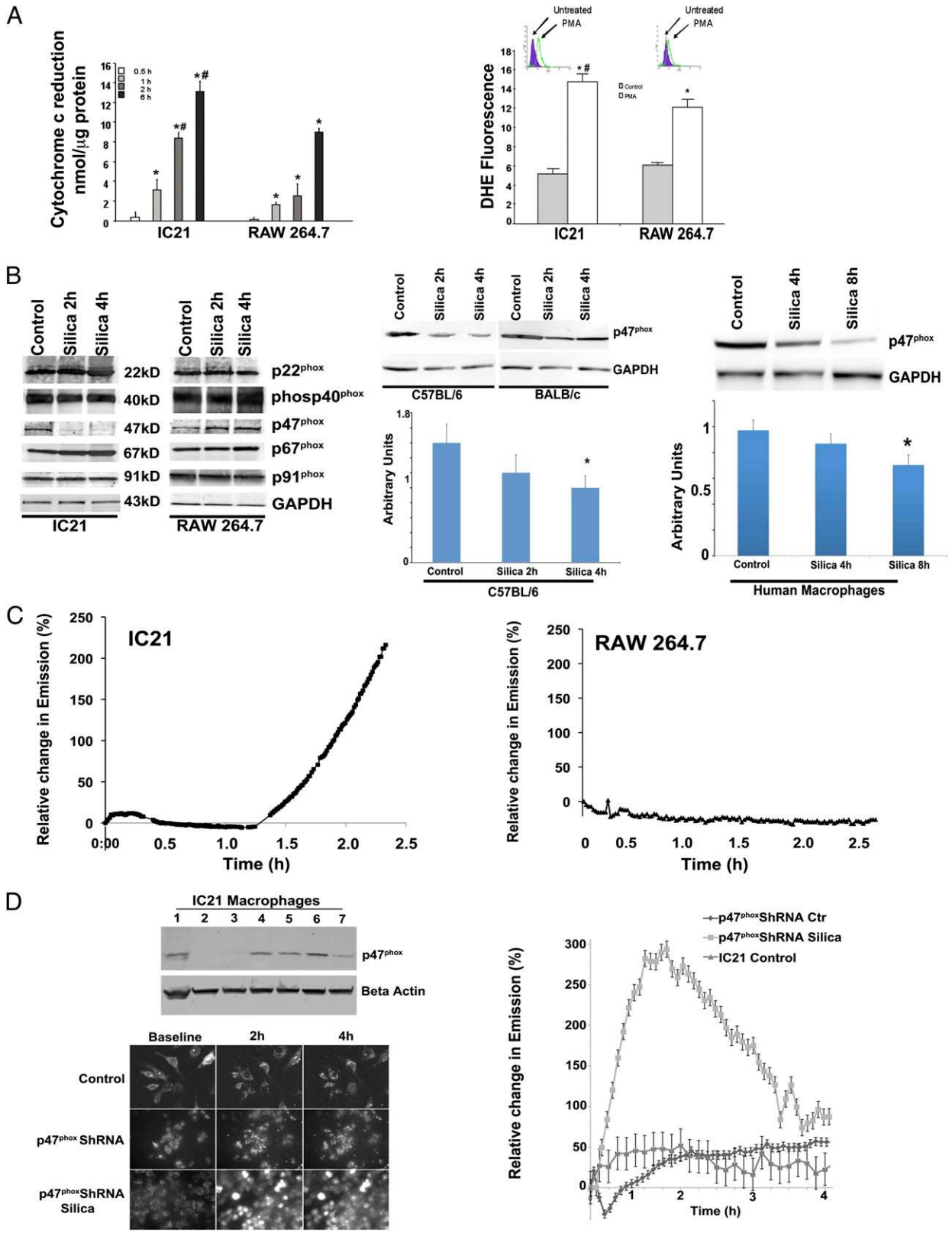

FIGURE 1. Mitochondria are a significant source of ROS in silica-exposed IC21 macrophages. (**A**) Following exposure to silica (*left panel*) or PMA (*right panel*), mitochondrial superoxide anion production increased in IC21 and RAW 264.7 macrophages, but the production was significantly greater in IC21 macrophages. Superoxide anion production was measured by cytochrome *c* (nmol/μg protein) reduction in response to silica (20 μg/cm^2) (*left panel*) or as changes in dihydroethidium fluorescence in response to PMA exposure (*right panel*). Basal level of cytochrome *c* reduction in untreated cells (5.3 nmol/μg protein in IC21 macrophages; 3.8 nmol/μg protein in RAW 264.7 macrophages) was subtracted from values obtained from silica-stimulated cells. Data are representative of duplicate samples obtained on three occasions. $^*p < 0.001$ versus control, $^{\#}p < 0.001$ versus RAW 264.7 cell line at same time point. (**B**) In response to silica, p47^{phox} protein decreased in IC21, but not in RAW 264.7, macrophages. Western blot analysis of NADPH oxidase proteins in IC21 and RAW 264.7 macrophages revealed reduced p47^{phox} expression in IC21 macrophages in response to silica (20 μg/cm^2) (*left panel*). Macrophages isolated from the bone marrow of C57BL/6 mice, but not from BALB/C mice (*middle panel*), as well as monocyte- (*Figure legend continues*)

peroxide anion production following silica exposure (Supplemental Fig. 1), indicating that a functional Phox is associated with diminished silica-induced mtROS production.

To provide more definitive evidence that a reduction in $p47^{phox}$ expression induces mtROS generation, IC21 macrophages were transfected with $p47^{phox}$-specific shRNA lentiviral particles, and reduced $p47^{phox}$ protein was confirmed by Western blotting (Fig. 1D). Subsequently, colonies of shRNA $p47^{phox}$ IC21 macrophages were established, and cells were treated with MitoSOX to document mtROS generation in vivo. Although baseline production of mtROS by nonstimulated shRNA $p47^{phox}$ IC21 macrophages is lower than that produced by control IC21 macrophages, these cells demonstrate a modest, but statistically greater, spontaneous increase in mtROS 2–4 h after incubation. In contrast, compared with control IC21 cells that only exhibit increased mtROS production after disappearance of $p47^{phox}$ protein (1.5 to 2 h after silica treatment), shRNA $p47^{phox}$ IC21 cells rapidly exhibit and have prolonged generation of mtROS in response to silica (Fig. 1D).

mtROS production is linked to cell death in silica-exposed macrophages

In response to silica, IC21, but not RAW 264.7, macrophages experience loss of mitochondrial membrane potential (Fig. 2A). Silica also induced a time-dependent decrease in the expression of the 39-kDa Complex I subunit, and Complex I enzymatic activity was inhibited to a greater degree in IC21 macrophages compared with RAW 264.7 macrophages (Fig. 2B).

Consistent with enhanced mtROS production, oxidized CL (CLox) increased more in IC21 macrophages compared with RAW 264.7 macrophages (Fig. 2C). In silica-exposed IC21 macrophages, C18:1/C8:2-OH/C18:1/C18:2-OOH at m/z 1500 were the predominant CL hydrolysis products (Fig. 2C). Silica exposure exclusively induced the formation of CL hydrolysis products—monolysocardiolipin (MLCL) and free fatty acids—in IC21 macrophages (Supplemental Fig. 2). Subsequently, electrospray ionization MS analysis identified the presence of nonoxidized MLCL [$(C_{18:2})_3$, $(C_{18:2})_2/(C_{18:1})_1$], and $[C_{18:2})_1/(C_{18:1})_2]$, as well as oxygenated species of $C_{18:2}$, in these cells (Fig. 2C, Supplemental Fig. 2).

Following silica exposure, IC21, but not RAW 264.7, macrophages released cytochrome *c* into their cytoplasm (Fig. 2D), which preceded the activation of executioner caspase 3 (Fig. 2E). Moreover, in response to silica, the number of apoptotic cells, with increased annexin V binding, and necrotic cells, with increased propidium iodide uptake, were greater in IC21 macrophages compared with RAW 264.7 macrophages (Fig. 2F).

TNFR1/Phox interaction is associated with diminished mtROS production by macrophages in response to silica

Macrophages differ in their ability to produce TNF in response to silica. RAW 264.7 macrophages release TNF in a dose- and time-dependent manner (Fig. 3A, 3B). In contrast, IC21 macrophages do not release TNF (Fig. 3C) following exposure to a range of silica concentrations (10–100 $\mu g/cm^2$) for up to 12 h when the mean level was 22 pg/ml. This is not due to a lack of capacity for TNF production inasmuch as IC21 macrophages secrete more TNF than do RAW 264.7 cells in response to LPS (Fig. 3D).

Similar to TNF production, RAW 26.7 macrophages exhibit greater expression of TNFR1 ($p < 0.05$) than do IC21 cells (Fig. 4A, 4B). Levels of cell-associated TNFR1 decreased in RAW 264.7 macrophages (Fig. 4A), but not in IC21 macrophages (Fig. 4B), in response to silica in a manner that parallels the secretion of TNF ligand (Fig. 3). In silica-exposed RAW 264.7 macrophages, the decreased cell-associated levels of TNFR1 were accompanied by increased TNFR1 in culture supernatant, indicating that the receptor is shed in response to silica by these cells (Fig. 4C). In contrast, TNFR1 in culture supernatants of IC21 macrophages was below the detection limit (data not shown).

TNFR1/Phox interaction involves the recruitment of TRADD to the death domain of the receptor, a process that takes place in the plasma membrane (28). To determine whether silica triggers interaction of RFK with TNFR1, we immunoprecipitated this receptor (pull down) from silica-exposed macrophages and analyzed the protein lysates for TRADD and RFK (Fig. 4D). Following silica exposure (1–2 h), RFK and TRADD coimmunoprecipitated on TNFR1 pull down from silica-exposed RAW 264.7 macrophages but not IC21 macrophages (Fig. 4D). Similarly, TNFR1 and RFK coimmunoprecipitate on TRADD pull-down proteins from silica-exposed RAW 264.7 cells (data not shown). Furthermore, the $p22^{phox}$ subunit of Phox was detected on TNFR1 (Fig. 4D) or TRADD (data not shown) pull-down proteins from silica-exposed RAW 264.7 macrophages. Therefore, in silica-exposed RAW 264.7 macrophages, RFK binds TRADD and links TNFR1 to the $p22^{phox}$ subunit of Phox.

TNF induces mtROS, and TNF is delivered to mitochondria where binding proteins have been documented (22, 29). Mitochondria from RAW 264.7, but not IC21, macrophages express TNFR1 (detected by a TNFR1 25-kDa C terminus peptide Ab) (Fig. 4E), suggesting that the mitochondrial location of TNFR1 takes place in association with receptor shedding (19). To determine the cell partition of TNFR1 in silica-exposed macrophages, we subjected cell lysates to sucrose density centrifugation. The largest proportion of TNFR1 in macrophages is located in heavy fractions (fractions 7–9) of the sucrose gradient in RAW 264.7 (Fig. 4F), but not in IC21 (data not shown), macrophages. In RAW 264.7 macrophages, silica induces the location of a small amount of TNFR1 to lighter fractions (4–6) in lipid domains enriched in caveolin 1 (Fig. 4F). ELISA analysis of proteins from sucrose density fractions 4–6 indicated that TNFR1 expression increased in these gradients as a percentage of total protein in response to silica (Fig. 4G).

To investigate the proteins associated with the gradient fraction that contained increased TNFR1 (fractions 4–6), the proteome of cell extracts from silica-treated RAW 264.7 cells were compared with that from untreated control RAW 264.7 cells. Following separation by PAGE (2-DE) and image analysis, 44 differentially expressed protein spots were identified (Fig. 4H). The gel spots were excised and subjected to in-gel trypsin digestion, followed by tandem MS analysis. Of the 44 spots identified, 43 yielded sig-

derived human macrophages (*right panel*), reacted to silica with significant reductions in $p47^{phox}$ expression. $^*p < 0.05$ versus control. (**C**) Following exposure to silica, mitochondrial superoxide anion production increased in both macrophage cell lines, but the production was greater in IC21 macrophages. Graphs illustrate the time course of MitoSOX emission by IC21 and RAW 264.7 cells ($n = 5$ tests/cell line, with 10 stage positions/test and six cells/stage position). (**D**) IC21 macrophages were infected with $p47^{phox}$-specific shRNA lentiviral particles also coding for puromycin resistance. Reduced $p47^{phox}$ expression was confirmed by Western blot (*upper left panel*), and shRNA $p47^{phox}$ IC21 cells (*lane 2*) were selected and expanded, under puromycin, for further experimentation. Photomicrographs (*lower left panel*, using original magnification ×10) and graph (*right panel*) illustrate the time-course of MitoSOX emission by IC21 and shRNA $p47^{phox}$ IC21 macrophages, alone or in response to silica (20 $\mu g/cm^2$) Data are representative of five different experiments with each experiment monitoring 10 stage positions that included six cells per stage position.

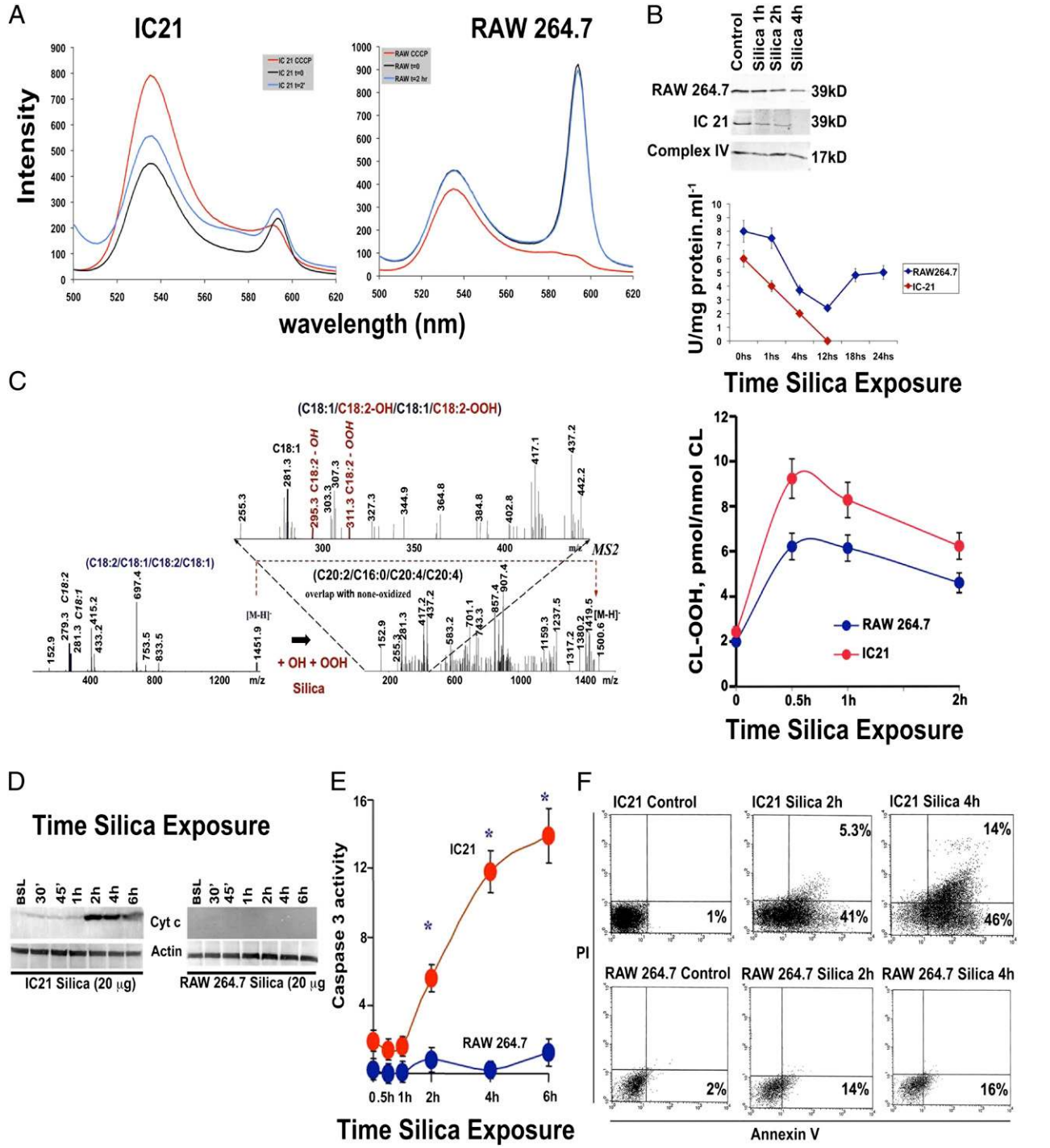

FIGURE 2. mtROS production is associated with mitochondrial injury, CL oxidation, and apoptosis in silica-exposed IC21 macrophages. (**A**) Mitochondrial membrane potential decreased in IC21, but not RAW 264.7, macrophages following silica exposure. Silica (20 μg/cm^2)-exposed IC21 and RAW 264.7 macrophages were incubated with JC-1 and analyzed by FACS. In response to silica, ~600-nm emission is low in IC21 macrophages, indicating that JC-1 cannot be processed to give an additional red fluorescent signal as a consequence of lost mitochondrial membrane potential. RAW 264.7 macrophages with normal mitochondrial membrane potential have preserved ~600-nm fluorescent signal. Data are from a representative test repeated three times. (**B**) Silica inhibits the enzymatic activity of mitochondrial Complex I. Mitochondria were isolated from IC21 and RAW 264.7 macrophages exposed to silica (20 μg/cm^2) for the indicated times, and Respiratory Complex I (39 kD subunit) abundance was determined by Western blot while using Complex IV expression as a loading control (*upper panel*); enzymatic activity (*lower panel*) was measured spectrophotometrically. In IC21 macrophages, but not in RAW 264.7 macrophages, silica induced a time-dependent decrease in the Complex I 39-kDa unit that was associated with progressive inhibition of the enzymatic activity of the complex. (**C**) Silica exposure induced time-dependent oxidation of CL in both macrophage cell lines, but the effects were significantly greater ($p < 0.001$) in IC21 macrophages, as determined by Amplex Red analysis. Silica exposure resulted in oxidation of primarily C18:2-containing molecular species of CL at m/z 1452, which corresponded to CL-OH and CL-OOH, with the dominant products of C18:1/C8:2-O/C18:1/C18:2-OO at m/z 1500, as determined by electrospray ionization MS analysis. (**D**) Cytochrome *c* was detected in cytosolic fractions of IC21 macrophages but not RAW 264.7 macrophages. Cells were exposed to 20 μg/cm^2 silica, and cytosolic fractions were analyzed by Western blot. (**E**) Silica exposure increased caspase 3 activity in IC21 macrophages. Caspase 3 activity was measured by colorimetric assay of cell extracts isolated from macrophages exposed to 20 μg/cm^2 silica. (**F**) In response to silica, the number of cells with increased annexin V binding and propidium iodide uptake was greater in IC21 (*Figure legend continues*)

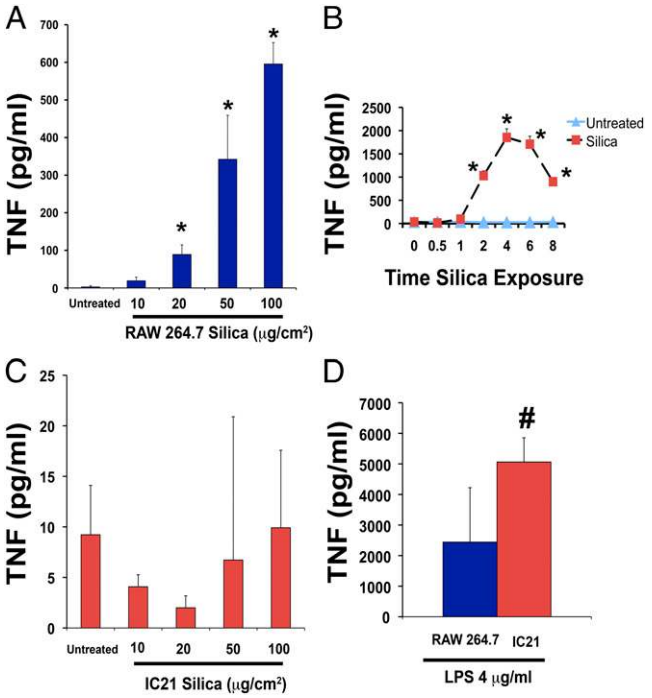

FIGURE 3. Silica induces TNF production in RAW 264.7, but not in IC21, macrophages. (**A**) TNF protein (pg/ml) released in cell-free supernatants of RAW 264.7 macrophage exposed to 10–100 μg/cm^2 silica for 2 h. (**B**) Time-course of TNF release by RAW 264.7 macrophages during silica exposure (50 μg/cm^2). (**C**) IC21 macrophages were exposed to 10–100 μg/cm^2 silica for 2 h. (**D**) IC21 macrophages exposed to 4 mg/ml LPS for 4 h can produce TNF. *$p < 0.001$ versus control-treated cells, #$p < 0.05$ versus LPS-treated RAW 264.7 cells.

nificant Mascot scores ≥ 50 ($p < 0.05$) and identified 41 distinct proteins (Supplemental Table I). The identified proteins were associated with antioxidant response, cytoskeleton and actin binding, inflammation and immunity, macrophage activation, metabolism and energy production, protein folding, and maintenance.

p47$^{phox-/-}$ mice experience enhanced silica-induced lung injury

To understand the implication of these observations in vivo, we exposed p47$^{phox-/-}$ and C57BL/6 mice to silica and compared the extent of lung injury, cytokine and fibrotic transcript levels, and the accumulation of collagen via analysis of trichrome staining. Lungs from both animals exhibit normal histology at baseline. In C57BL/6 mice, silica predominantly induced lesions that encased the terminal bronchiolar–alveolar duct regions (Fig. 5A). These lesions resembled the silicotic nodule observed in humans and consisted of dense accumulations of peribronchiolar inflammatory cells and increased staining with trichrome blue, suggestive of localized collagen deposition. In contrast, p47$^{phox-/-}$ mice predominantly reacted to silica with accumulation of "foamy macrophages" and multinucleated giant cells in airspaces and alveolar regions, and the accumulation of collagen is diffuse rather than localized to the well-defined peribronchiolar nodules observed in C57BL/6 mice (Fig. 5A). Quantitative analysis of the trichrome staining showed that, following silica exposure, p47$^{phox-/-}$ mice demonstrate statistically significantly ($p < 0.05$) greater accumulation of collagen in their lungs and >20% of the lung surface stained positive for collagen 28 d after silica exposure (Fig. 5B). These inflammatory and fibrotic responses were accompanied by significantly greater increases in TNF, IL-6, TGFβ, and collagen, type 1, α1 mRNA levels in the lungs of silica-exposed p47$^{phox-/-}$ mice compared with silica-exposed C57BL/6 mice (Fig. 5B).

Discussion

The main finding of the current work is that macrophages can differ in innate immune responses to silica. Macrophages with the ability to survive silica particles generate more TNF and less mtROS. In silica-sensitive IC21 macrophages, inhibition of p47^{phox} expression, lack of TNFR1/phox interaction, and absence of mitochondrial TNFR1 were associated with increased mtROS generation and cell death in response to silica. Similar to IC21 macrophages, p47$^{phox-/-}$ macrophages demonstrate enhanced mtROS production, and p47$^{phox-/-}$ mice experience exacerbated lung injury when challenged with silica particles.

Supporting the importance of a functional Phox in limiting silicosis, p47$^{phox-/-}$ macrophages exhibit a reduced ability to clear bacteria (30, 31). p47$^{phox-/-}$ mice develop progressive crystalline macrophage pneumonia and exhibit higher levels of Th1 (including TNF), Th2, and Th17 secretions in lung attributed to an intrinsic abnormality in macrophage activation (13). Our data indicate that this response is also associated with enhanced mtROS production in macrophages. The mechanisms responsible for mtROS production in macrophages are not fully understood, but they are likely to involve the recruitment of mitochondria to phagosomes and interactions with TRAF6. In addition, inhibition of autophagy may lead to the retention of dysfunctional mitochondria (10, 32). The current work links the generation of mtROS to mitochondrial injury, as demonstrated by induced silica CLox production and reduced activity of mitochondrial Complex I (Fig. 2). CL localizes to contact sites of mitochondria where it provides stability to respiratory complexes, anchors caspase-8, and targets BH3 interacting domain death agonist (BID) (33). CL's interactions with cytochrome *c* result in partial unfolding of this protein, making its heme catalytic site accessible to H_2O_2 (24). During cell death, cytochrome *c* assumes significant peroxidase activity, and cytochrome *c*/CL complexes generate CL hydroperoxides (24).

CL function depends on the presence of mature CL that is produced by the combined action of phospholipase A2 and the CL transacylase, tafazzin, which removes one acyl chain to generate MLCL (33). Importantly, enhanced phospholipase A2 activity has been observed in silica-exposed macrophages (34). Consequently, accumulation of CLox products, as observed in silica-exposed IC21 macrophages, implicates mtROS production and dysfunction of mitochondrial respiratory Complex I (Fig. 2). Complex I is a site of electron addition to oxygen that generates superoxide anion, which leads to H_2O_2 formation (35, 36). Consistent with this mechanism, human CMV prevents rotenone-induced apoptosis of infected cells by producing β2.7 RNA that stabilizes Complex I, preserving mitochondrial membrane potential and ATP production required for cell survival of infected host cells (37).

macrophages compared with RAW 264.7 macrophages. FACS colocalization of annexin V binding and propidium iodine uptake on silica (20 μg/cm^2)-exposed macrophage populations. Each panel depicts data gathered from 10,000 individual cells. Horizontal axis depicts fluorescein-labeled annexin V, and the vertical axis shows binding of propidium iodide fluorescence. Data are representative of five independent tests. *$p < 0.001$ versus RAW264.7 macrophage cell line.

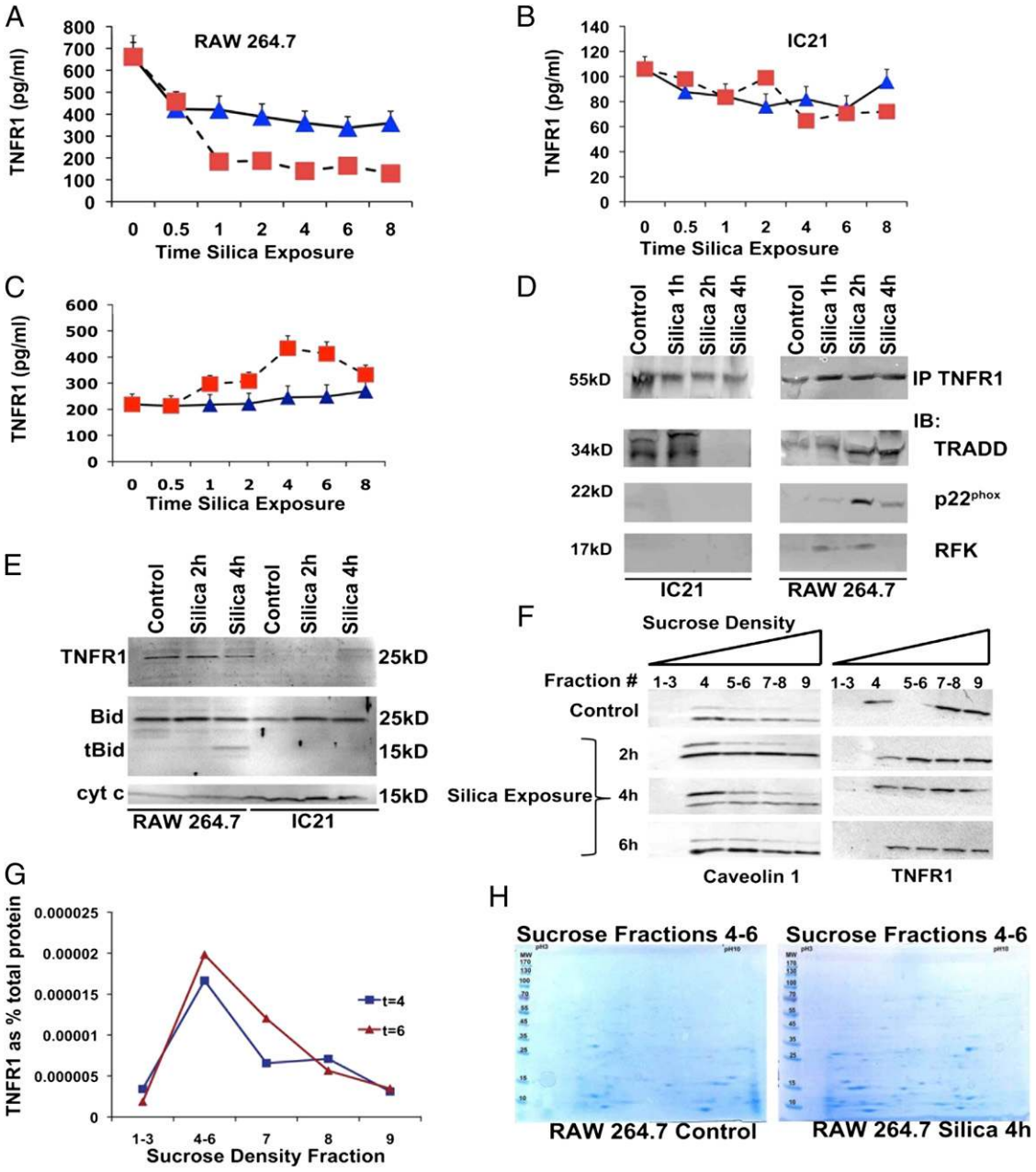

FIGURE 4. Silica alters TNFR1 expression and cell distribution and induces TNFR1/Phox interaction in silica-exposed RAW 264.7 macrophages. TNFR1 protein measured by ELISA in whole-cell lysates (**A** and **B**) or culture supernatants (**C**) extracted from RAW 264.7 (A and C) or IC21 (B) macrophages following silica (20 $\mu g/cm^2$) exposure (0–8 h). ■, silica-exposed cells; ▲, control-treated cells. (**D**) In RAW 264.7 macrophages, silica induces expression of RFK, which coimmunoprecipitates with TRADD and $p22^{phox}$. TNFR1 immunoprecipitates (IP) from IC21 or RAW 264.7 macrophages (5×10^8 cells), exposed to silica (20 $\mu g/cm^2$) for 0–4 h, were immunoblotted with Abs specific to TRADD, RFK, and $p22^{phox}$. Results are representative of three independent exposures. (**E**) TNFR1 is expressed in mitochondria from silica-exposed-RAW 264.7 macrophages but not IC21 macrophages. Mitochondria were isolated from 1×10^9 RAW 264.7 and IC21 macrophages following silica exposure, and TNFR1 and tBid localization were analyzed by Western blotting using Abs against TNFR1 or tBid. Cytochrome *c* was used as a mitochondrial marker and loading control. Twice the concentration of proteins (100 μg) loaded in lanes from IC21 samples. Gel is representative of four experiments. (**F**) Silica exposure induces TNFR1 endocytosis in caveolin-containing rafts. Following silica (20 $\mu g/cm^2$) exposure for 0–6 h, RAW 264.7 macrophages (5×10^8 cells) were lysed and subjected to a 45% sucrose gradient, as described in *Materials and Methods*. Gels from each gradient were stained with Abs against TNFR1 or caveolin. (**G**) TNFR1 protein measured by ELISA in sucrose gradients isolated from RAW 264.7 macrophages 4 h after silica exposure. (**H**) Proteins from specific sucrose density gradients were resolved by two-dimensional gel electrophoresis and subjected to MALDI-TOF analysis to identify proteins that were differentially expressed in the gradients following silica exposure (Supplemental Table I).

TNF antagonism was proposed as a therapeutic measure to treat silicosis (16). However, TNF makes an important contribution toward the survival of macrophages to silica. Previously, we found that inhibition of TNF-mediated NF-κB activation significantly enhanced silica-induced apoptosis in RAW 264.7 macrophages and worsened silica-induced lung injury in mice (1, 27). The current work demonstrates that macrophages differ in their secretion of TNF in response to silica and that TNF expression in RAW 264.7 macrophages triggers TNFR1-signaling events that diminish ROS production.

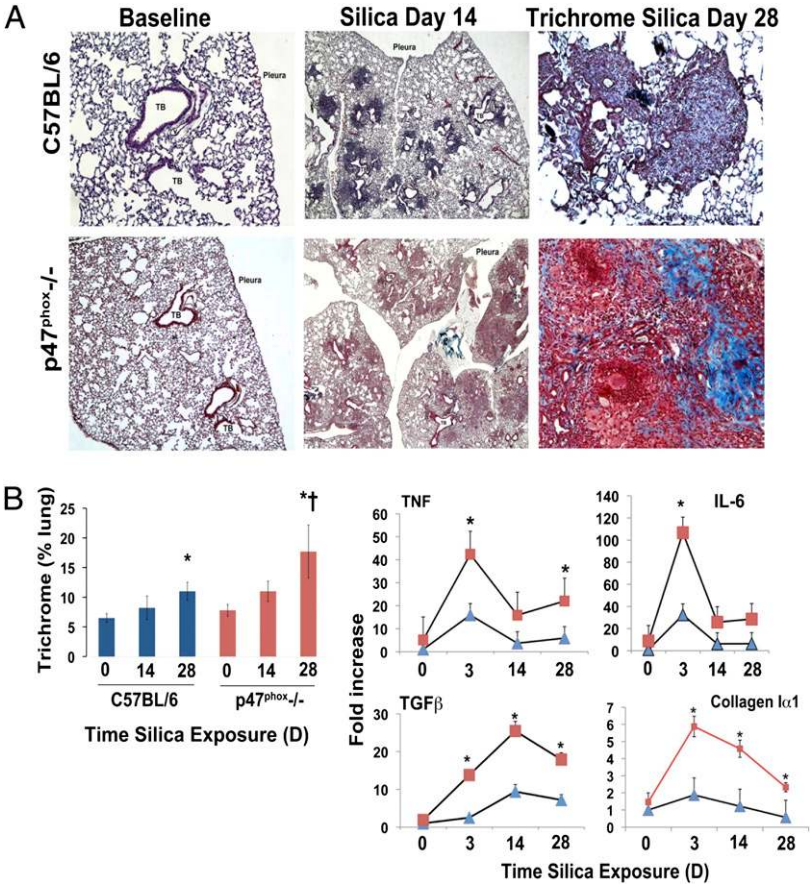

FIGURE 5. $p47^{phox}$ deficiency enhances silica-induced lung injury. (**A**) Lung photomicrographs (original magnifications ×4 [*middle panel*] and ×10 [*right panel*]) obtained from C57BL/6 (strain-matched controls, *left panel*, original magnification ×4) or $p47^{phox-/-}$ mice 0–28 d after intratracheal crystalline silica (0.2 g/kg) administration. In C57BL/6 mice, silica predominantly induced lesions that encased the terminal bronchiolar–alveolar duct region, and the nodule-like lesions show increased staining with trichrome blue, consistent with localized collagen deposition 28 d after silica exposure. In contrast, $p47^{phox-/-}$ mice react to silica with diffuse parenchymal accumulation of foamy macrophages and multinucleated giant cells and exhibit diffuse parenchymal deposition of collagen. (**B**) Quantitative analysis of trichrome staining demonstrates that both mouse strains accumulate significant amounts of collagen in their lungs compared with control (*$p < 0.05$), but the accumulation is statistically significantly greater ($^{\dagger}p < 0.05$) in the lungs of p47phox$^{-/-}$ mice. Enhanced expression of inflammatory cytokines (TNF, IL-6), and fibrotic-related (TGFβ and collagen type 1, α 1) transcripts were measured by real-time PCR in the lungs as a function of time following intratracheal exposure to crystalline silica (0.2 mg/kg). Data are mean (± SE) fold increase normalized to RPL32 (Mm02528467_g1) gene expression as internal control (n = 5 mice/time point). Squares represent data from $p47^{phox-/-}$ and triangles represent data from C57BL/6 mice. *$p < 0.001$ versus C57BL/6 mouse strain.

Previously, TNFR1's interaction with NADPH was described in HeLa cells as a regulatory mechanism to stimulate TNF-mediated ROS production (21). In RAW 264.7 macrophages, recombinant RFK phosphorylates riboflavin to produce flavin mononucleotide, a rate-limiting step in the synthesis of FAD, an essential prosthetic group of NADPH oxidase (21). TNFR1/Phox interaction appears to be very selective, because RFK-mediated bridging of TNFR1 and $p22^{phox}$ is required for TNF, but not TLR, receptor-induced ROS production (21). The absence of TNF production by IC21 macrophages and the lack of RFK recruitment to TNFR1 in these cells in response to silica suggest that this interaction may be a key regulator of Phox-mediated ROS production by macrophages, and its absence would force these cells to use mitochondria as an alternative source for ROS, thereby compromising cell survival.

Recruitment of TRADD is fundamental to the interaction of TNFR1 with NADPH oxidase. TRADD is capable of simultaneously inducing prosurvival, NF-κB, or apoptotic signals and BID cleavage (38). Aggregation of TRADD to establish DISC formation is followed by TNFR1 endocytosis to *trans*-Golgi vesicles (39). Ledgerwood et al. (29) used immunoelectron microscopy and Western blotting techniques to demonstrate that TNF is delivered to mitochondria where it interacts with a 60-kDa protein in the inner mitochondrial membrane. Recently, Eum et al. (22) reported that TNF treatment of hepatocytes induces the appearance of TNFR1 and caspase 8, but not TRADD, in mitochondria. Consistent with these observations, the current work found the expression of TNFR1, caspase 8, and BID in the mitochondria of RAW 264.7, but not IC21, macrophages (Fig. 4). In addition, we found that silica altered the expression of TNFR1 and induced cytoplasmic trafficking of TNFR1 in RAW 264.7 cells.

The potential role of TNFR1 in limiting mtROS production is not fully understood. It is not clear whether macrophages express NADPH oxidase in mitochondria; however, because TRADD does not appear to translocate to mitochondria, it is unlikely that TNFR1 interacts with this protein in the same way as cell membrane–bound Phox at this site. In RAW 264.7 macrophages, silica triggers TNFR1 traffic in caveolin-containing domains, and the receptor is enriched in specific subcellular locations, as suggested by the analysis of TNFR1 expression in sucrose density fractions. Proteomic analysis of RAW 264.7 macrophages suggests that TNFR1-enriched fractions are also enriched in proteins mediating the antioxidant, inflammatory, cytoskeletal, and metabolic functions of macrophages. Of particular relevance, antioxidants are likely to be protective and included NmrA-like family domain containing 1, a NADPH oxidase sensor that can decrease NO synthesis by association with argininosuccinate synthetase and, thereby, increase cell survival (40). In addition, annexin A1 can inhibit inducible NO synthase expression in macrophages and can limit phospholipase A2 activity (41). The latter may limit MLCL formation (42) and would be protective to the RAW 264.7 macrophage during silica challenge. Among the inflammatory mediators, macrophage migration inhibitory factor can enhance TNF production following LPS stimulation and macrophage survival (43). Lastly, this fraction was enriched in cytoskeletal proteins and in mitochondrial (as expected) and cytosolic glycolytic enzymes, suggesting a recruitment of a multienzyme energetic cluster complex that enhances ATP maintenance and promotes cell survival (44).

Overall, the current data indicate that $p47^{phox}$ deficiency or absence of TNF production by macrophages results in enhanced production of mtROS that is linked to cell death and inflammation in response to silica. Therefore, inhibition of macrophage TNF production may not constitute an appropriate clinical target in silicosis.

Disclosures

The authors have no financial conflicts of interest.

References

1. Di Giuseppe, M., F. Gambelli, G. W. Hoyle, G. Lungarella, S. M. Studer, T. Richards, S. Yousem, K. McCurry, J. Dauber, N. Kaminski, et al. 2009. Systemic inhibition of NF-kappaB activation protects from silicosis. *PLoS ONE* 4: e5689.
2. Dostert, C., V. Pétrilli, R. Van Bruggen, C. Steele, B. T. Mossman, and J. Tschopp. 2008. Innate immune activation through Nalp3 inflammasome sensing of asbestos and silica. *Science* 320: 674–677.
3. Cassel, S. L., S. C. Eisenbarth, S. S. Iyer, J. J. Sadler, O. R. Colegio, L. A. Tephly, A. B. Carter, P. B. Rothman, R. A. Flavell, and F. S. Sutterwala. 2008. The Nalp3 inflammasome is essential for the development of silicosis. *Proc. Natl. Acad. Sci. USA* 105: 9035–9040.
4. Hornung, V., F. Bauernfeind, A. Halle, E. O. Samstad, H. Kono, K. L. Rock, K. A. Fitzgerald, and E. Latz. 2008. Silica crystals and aluminum salts activate the NALP3 inflammasome through phagosomal destabilization. *Nat. Immunol.* 9: 847–856.
5. Costantini, L. M., R. M. Gilberti, and D. A. Knecht. 2011. The phagocytosis and toxicity of amorphous silica. *PLoS ONE* 6: e14647.
6. Beamer, C. A., and A. Holian. 2008. Silica suppresses Toll-like receptor ligand-induced dendritic cell activation. *FASEB J.* 22: 2053–2063.
7. Giordano, G., S. van den Brule, S. Lo Re, P. Triqueneaux, F. Uwambayinema, Y. Yakoub, I. Couillin, B. Ryffel, T. Michiels, J. C. Renauld, D. Lison, and F. Huaux. 2010. Type I interferon signaling contributes to chronic inflammation in a murine model of silicosis. *Toxicol. Sci.* 116: 682–692.
8. Lambeth, J. D. 2004. NOX enzymes and the biology of reactive oxygen. *Nat. Rev. Immunol.* 4: 181–189.
9. Naik, E., and V. M. Dixit. 2011. Mitochondrial reactive oxygen species drive proinflammatory cytokine production. *J. Exp. Med.* 208: 417–420.
10. West, A. P., I. E. Brodsky, C. Rahner, D. K. Woo, H. Erdjument-Bromage, P. Tempst, M. C. Walsh, Y. Choi, G. S. Shadel, and S. Ghosh. 2011. TLR signalling augments macrophage bactericidal activity through mitochondrial ROS. *Nature* 472: 476–480.
11. Segal, B. H., W. Han, J. J. Bushey, M. Joo, Z. Bhatti, J. Feminella, C. G. Dennis, R. R. Vethanayagam, F. E. Yull, M. Capitano, et al. 2010. NADPH oxidase limits innate immune responses in the lungs in mice. *PLoS ONE* 5: e9631.
12. Zhang, W.-J., H. Wei, and B. Frei. 2009. Genetic deficiency of NADPH oxidase does not diminish, but rather enhances, LPS-induced acute inflammatory responses in vivo. *Free Radic. Biol. Med.* 46: 791–798.
13. Liu, Q., L. I. Cheng, L. Yi, N. Zhu, A. Wood, C. M. Changpriroa, J. M. Ward, and S. H. Jackson. 2009. p47phox deficiency induces macrophage dysfunction resulting in progressive crystalline macrophage pneumonia. *Am. J. Pathol.* 174: 153–163.
14. Zhang, W. J., H. Wei, Y. T. Tien, and B. Frei. 2011. Genetic ablation of phagocytic NADPH oxidase in mice limits TNFα-induced inflammation in the lungs but not other tissues. *Free Radic. Biol. Med.* 50: 1517–1525.
15. Scarfì, S., M. Magnone, C. Ferraris, M. Pozzolini, F. Benvenuto, U. Benatti, and M. Giovine. 2009. Ascorbic acid pre-treated quartz stimulates TNF-alpha release in RAW 264.7 murine macrophages through ROS production and membrane lipid peroxidation. *Respir. Res.* 10: 25.
16. Piguet, P. F., M. A. Collart, G. E. Grau, A. P. Sappino, and P. Vassalli. 1990. Requirement of tumour necrosis factor for development of silica-induced pulmonary fibrosis. *Nature* 344: 245–247.
17. Kim, Y. S., M. J. Morgan, S. Choksi, and Z. G. Liu. 2007. TNF-induced activation of the Nox1 NADPH oxidase and its role in the induction of necrotic cell death. *Mol. Cell* 26: 675–687.
18. Ortiz, L. A., J. Lasky, E. Gozal, V. Ruiz, G. Lungarella, E. Cavarra, A. R. Brody, M. Friedman, A. Pardo, and M. Selman. 2001. Tumor necrosis factor receptor deficiency alters matrix metalloproteinase 13/tissue inhibitor of metalloproteinase 1 expression in murine silicosis. *Am. J. Respir. Crit. Care Med.* 163: 244–252.
19. Rowlands, D. J., M. N. Islam, S. R. Das, A. Huertas, S. K. Quadri, K. Horiuchi, N. Inamdar, M. T. Emin, J. Lindert, V. S. Ten, et al. 2011. Activation of TNFR1 ectodomain shedding by mitochondrial Ca2+ determines the severity of inflammation in mouse lung microvessels. *J. Clin. Invest.* 121: 1986–1999.
20. Roca, F. J., and L. Ramakrishnan. 2013. TNF dually mediates resistance and susceptibility to mycobacteria via mitochondrial reactive oxygen species. *Cell* 153: 521–534.
21. Yazdanpanah, B., K. Wiegmann, V. Tchikov, O. Krut, C. Pongratz, M. Schramm, A. Kleinridders, T. Wunderlich, H. Kashkar, O. Utermöhlen, et al. 2009. Riboflavin kinase couples TNF receptor 1 to NADPH oxidase. *Nature* 460: 1159–1163.
22. Eum, H. A., R. Vallabhaneni, Y. Wang, P. A. Loughran, D. B. Stolz, and T. R. Billiar. 2011. Characterization of DISC formation and TNFR1 translocation to mitochondria in TNF-α-treated hepatocytes. *Am. J. Pathol.* 179: 1221–1229.
23. Bulua, A. C., A. Simon, R. Maddipati, M. Pelletier, H. Park, K. Y. Kim, M. N. Sack, D. L. Kastner, and R. M. Siegel. 2011. Mitochondrial reactive oxygen species promote production of proinflammatory cytokines and are elevated in TNFR1-associated periodic syndrome (TRAPS). *J. Exp. Med.* 208: 519–533.
24. Kagan, V. E., V. A. Tyurin, J. Jiang, Y. Y. Tyurina, V. B. Ritov, A. A. Amoscato, A. N. Osipov, N. A. Belikova, A. A. Kapralov, V. Kini, et al. 2005. Cytochrome c acts as a cardiolipin oxygenase required for release of proapoptotic factors. *Nat. Chem. Biol.* 1: 223–232.
25. Davies, J. Q., and S. Gordon. 2005. Isolation and culture of murine macrophages. *Methods Mol. Biol.* 290: 91–103.
26. Vogt, G., and C. Nathan. 2011. In vitro differentiation of human macrophages with enhanced antimycobacterial activity. *J. Clin. Invest.* 121: 3889–3901.
27. Gambelli, F., P. Di, X. Niu, M. Friedman, T. Hammond, D. W. Riches, and L. A. Ortiz. 2004. Phosphorylation of tumor necrosis factor receptor 1 (p55) protects macrophages from silica-induced apoptosis. *J. Biol. Chem.* 279: 2020–2029.
28. Jones, S. J., E. C. Ledgerwood, J. B. Prins, J. Galbraith, D. R. Johnson, J. S. Pober, and J. R. Bradley. 1999. TNF recruits TRADD to the plasma membrane but not the trans-Golgi network, the principal subcellular location of TNF-R1. *J. Immunol.* 162: 1042–1048.
29. Ledgerwood, E. C., J. B. Prins, N. A. Bright, D. R. Johnson, K. Wolfreys, J. S. Pober, S. O'Rahilly, and J. R. Bradley. 1998. Tumor necrosis factor is delivered to mitochondria where a tumor necrosis factor-binding protein is localized. *Lab. Invest.* 78: 1583–1589.
30. Sanmun, D., E. Witasp, S. Jitkaew, Y. Y. Tyurina, V. E. Kagan, A. Ahlin, J. Palmblad, and B. Fadeel. 2009. Involvement of a functional NADPH oxidase in neutrophils and macrophages during programmed cell clearance: implications for chronic granulomatous disease. *Am. J. Physiol. Cell Physiol.* 297: C621–C631.
31. Sadikot, R. T., H. Zeng, F. E. Yull, B. Li, D. S. Cheng, D. S. Kernodle, E. D. Jansen, C. H. Contag, B. H. Segal, S. M. Holland, et al. 2004. p47phox deficiency impairs NF-κ B activation and host defense in *Pseudomonas* pneumonia. *J. Immunol.* 172: 1801–1808.
32. Zhou, J., S. Zhang, X. Zhao, and T. Wei. 2008. Melatonin impairs NADPH oxidase assembly and decreases superoxide anion production in microglia exposed to amyloid-beta1-42. *J. Pineal Res.* 45: 157–165.
33. Gonzalvez, F., Z. T. Schug, R. H. Houtkooper, E. D. MacKenzie, D. G. Brooks, R. J. Wanders, P. X. Petit, F. M. Vaz, and E. Gottlieb. 2008. Cardiolipin provides an essential activating platform for caspase-8 on mitochondria. *J. Cell Biol.* 183: 681–696.
34. Nakajima, T., M. Ito, U. Tchoua, H. Tojo, and M. Hashimoto. 2000. Phospholipase A2-mediated superoxide production of murine peritoneal macrophages induced by chrysotile stimulation. *Int. J. Biochem. Cell Biol.* 32: 779–787.
35. Koopman, W. J., L. G. Nijtmans, C. E. Dieteren, P. Roestenberg, F. Valsecchi, J. A. Smeitink, and P. H. Willems. 2010. Mammalian mitochondrial complex I: biogenesis, regulation, and reactive oxygen species generation. *Antioxid. Redox Signal.* 12: 1431–1470.
36. Murphy, M. P. 2009. How mitochondria produce reactive oxygen species. *Biochem. J.* 417: 1–13.
37. Reeves, M. B., A. A. Davies, B. P. McSharry, G. W. Wilkinson, and J. H. Sinclair. 2007. Complex I binding by a virally encoded RNA regulates mitochondria-induced cell death. *Science* 316: 1345–1348.
38. Micheau, O., and J. Tschopp. 2003. Induction of TNF receptor I-mediated apoptosis via two sequential signaling complexes. *Cell* 114: 181–190.
39. Schneider-Brachert, W., V. Tchikov, J. Neumeyer, M. Jakob, S. Winoto-Morbach, J. Held-Feindt, M. Heinrich, O. Merkel, M. Ehrenschwender, D. Adam, et al. 2004. Compartmentalization of TNF receptor 1 signaling: internalized TNF receptosomes as death signaling vesicles. *Immunity* 21: 415–428.
40. Zhao, Y., J. Zhang, H. Li, Y. Li, J. Ren, M. Luo, and X. Zheng. 2008. An NADPH sensor protein (HSCARG) down-regulates nitric oxide synthesis by association with argininosuccinate synthetase and is essential for epithelial cell viability. *J. Biol. Chem.* 283: 11004–11013.
41. Perretti, M., and F. D'Acquisto. 2009. Annexin A1 and glucocorticoids as effectors of the resolution of inflammation. *Nat. Rev. Immunol.* 9: 62–70.
42. Danos, M., W. A. Taylor, and G. M. Hatch. 2008. Mitochondrial monolysocardiolipin acyltransferase is elevated in the surviving population of H9c2 cardiac myoblast cells exposed to 2-deoxyglucose-induced apoptosis. *Biochem. Cell Biol.* 86: 11–20.
43. Lue, H., M. Thiele, J. Franz, E. Dahl, S. Speckgens, L. Leng, G. Fingerle-Rowson, R. Bucala, B. Lüscher, and J. Bernhagen. 2007. Macrophage migration inhibitory factor (MIF) promotes cell survival by activation of the Akt pathway and role for CSN5/JAB1 in the control of autocrine MIF activity. *Oncogene* 26: 5046–5059.
44. Seth, R., J. Keeley, G. Abu-Ali, S. Crook, D. Jackson, and M. Ilyas. 2009. The putative tumour modifier gene ATP5A1 is not mutated in human colorectal cancer cell lines but expression levels correlate with TP53 mutations and chromosomal instability. *J. Clin. Pathol.* 62: 598–603.